

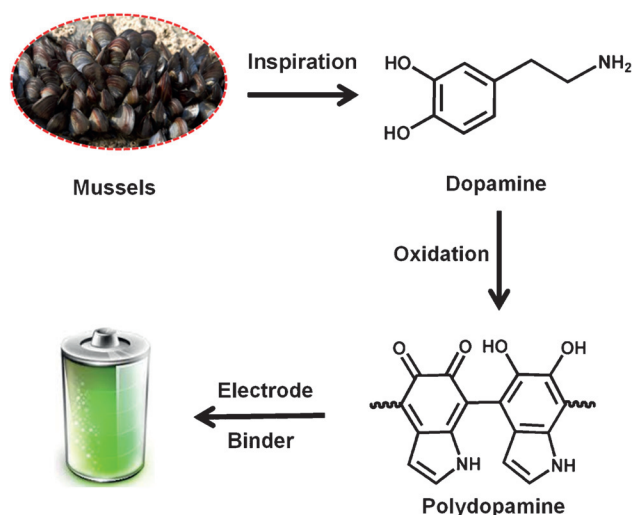
# A Biodegradable Polydopamine-Derived Electrode Material for High-Capacity and Long-Life Lithium-Ion and Sodium-Ion Batteries

Tao Sun, Zong-jun Li, Heng-guo Wang, Di Bao, Fan-lu Meng, and Xin-bo Zhang\*

**Abstract:** Polydopamine (PDA), which is biodegradable and is derived from naturally occurring products, can be employed as an electrode material, wherein controllable partial oxidation plays a key role in balancing the proportion of redox-active carbonyl groups and the structural stability and conductivity. Unexpectedly, the optimized PDA derivative endows lithium-ion batteries (LIBs) or sodium-ion batteries (SIBs) with superior electrochemical performances, including high capacities ( $1818 \text{ mAh g}^{-1}$  for LIBs and  $500 \text{ mAh g}^{-1}$  for SIBs) and good stable cyclabilities (93 % capacity retention after 580 cycles for LIBs; 100 % capacity retention after 1024 cycles for SIBs), which are much better than those of their counterparts with conventional binders.

Organic battery electrode materials derived from renewable and abundant resources are crucial for “green” batteries and can replace unsustainable active components in electrochemical devices, including lithium-ion or sodium-ion batteries (LIBs or SIBs).<sup>[1]</sup> Although exciting progress has been made in the field, the large-scale applications of such materials are still hindered by many challenges, including low specific capacity, short cycle life, and poor rate capability.<sup>[2]</sup> Furthermore, the synthesis of most of the organic electrode materials involves expensive and toxic agents.<sup>[3–6]</sup> Therefore, the use of a facile and green strategy for the development of high-performance organic materials with high capacities and good cyclic stabilities from renewable resources is of significant importance and remains a challenge.

Inspired by physiological processes based on ion transport and energy conversion of functional biomolecules, the functionalization of naturally occurring biomolecules inspired us to develop biocompatible organic electrode materials.<sup>[7–9]</sup> As one of the most important neurotransmitters in the central nervous system, dopamine (DA) plays an essential role in the regulation of physiological processes.<sup>[10]</sup> Interestingly, DA can be oxidized to *o*-benzoquinone by electron transfer (Scheme S1 in the Supporting Information), and the resulting catechol/*o*-benzoquinone redox system plays a fundamental role in Parkinson’s disease.<sup>[10]</sup> Therefore, polydopamine (PDA) could be an ideal redox-active biomolecule-based electrode material provided that the proton is replaced with lithium/sodium ions. Interestingly, the oxygen atom in *o*-benzoquinone is suitably located for coordination to lithium/sodium ions (Scheme 1).<sup>[11,12]</sup> It should be noted



**Scheme 1.** Preparation of the bifunctional electrode/binder material.

that, although a higher *o*-benzoquinone content in PDA could provide more redox-active sites and thus a higher capacity, excessive oxidation or reduction would compromise the electronic conductivity and thus the electrochemical performance. Therefore, oxidation state optimization is crucial for the use of PDA in sustainable and biocompatible electrode materials.

In conventional battery electrodes, the necessary addition of an insulating, inactive, and easily swelling polymeric binder would inevitably result in irreversible capacity losses and poor cycling stability.<sup>[13]</sup> The construction of binder-free electrodes

\* T. Sun, D. Bao, F. L. Meng, Prof. X. B. Zhang  
State Key Laboratory of Rare Earth Resource Utilization  
Changchun Institute of Applied Chemistry  
Chinese Academy of Sciences, Changchun  
130022 (P.R. China)  
E-mail: xbzhang@ciac.ac.cn

Z. J. Li  
State Key Laboratory of Electroanalytical Chemistry, Changchun  
Institute of Applied Chemistry, Chinese Academy of Sciences  
Changchun, 130022 (P.R. China)

H. G. Wang  
School of Materials Science and Engineering  
Changchun University of Science and Technology  
Changchun 130022 (P.R. China)

T. Sun  
University of Chinese Academy of Sciences  
Beijing, 100049 (P.R. China)

Supporting information and the ORCID identification number(s) for the author(s) of this article can be found under <http://dx.doi.org/10.1002/anie.201604519>.

could thus be a promising strategy; however, the available fabrication methods suffer drawbacks such as the requirement of special equipment, as well as complicated, and energy and time-consuming preparation. Interestingly, the existence of PDA (with a catechol group) is mainly responsible for the strong adhesion properties of many marine or freshwater bivalves.<sup>[14]</sup> Therefore, theoretically, PDA could be employed as both electrode and redox-active binder material. To the best of our knowledge, there is no report to date on the use of PDA as electrode or binder materials for LIBs and SIBs, or as bifunctional electrode/binder materials.

Inspired by the redox activity of catechol/*o*-benzoquinone in DA for neuronal communication, we chose PDA as both electrode and binder material for LIBs and SIBs, wherein electrons are transferred from catechol to *o*-benzoquinone to provide quinone-rich PDA in the optimized oxidation state through the rational manipulation of oxidant and heat treatment. Unexpectedly, the obtained PDA exhibits excellent electrochemical performance, including a high specific capacity (1818 mAh g<sup>-1</sup> and 500 mAh g<sup>-1</sup>) and excellent cycling stability (1414 mAh g<sup>-1</sup> after 580 cycles with a capacity retention at 93% under 500 mA g<sup>-1</sup> for LIBs, 500 mAh g<sup>-1</sup> after 1024 cycles with a capacity retention at 100% under 50 mA g<sup>-1</sup> for SIBs).

PDA was synthesized by using (NH<sub>4</sub>)<sub>2</sub>S<sub>2</sub>O<sub>8</sub> (APS) and the final product was dried at 180 °C in air for 24 h.<sup>[15–17]</sup> Thermogravimetric analysis (TGA) of the obtained amorphous PDA microspheres (Figures S1, S2) reveals that there is no weight loss from 100 to 200 °C, thus guaranteeing the structural stability during heat treatment. To tune the degree of oxidation and the electrochemical properties of PDA, we fabricated a series of samples with APS/DA ratios varying from 1:1 to 4:1, which were labeled as O-PDA-1 to O-PDA-4, respectively (detailed procedures and analyses are given in the Supporting Information). Various characterization methods were applied to confirm the structure of the PDA. Immediately after the addition of APS, the UV/Vis spectrum shows an absorption peak at around 350 nm, which corresponds to the oxidation of catechol to *o*-benzoquinone (Figure S3).<sup>[18]</sup> According to the <sup>13</sup>C solid-state CP-MAS NMR spectrum (Figure S4),<sup>[19–21]</sup> the resonance at 30–40 ppm may be ascribed to the carbon atoms of the partially saturated five membered rings. Peaks corresponding to carbonyl C atoms are found at about 160–180 ppm. The signals at 120 ppm that correspond to quaternary carbon atoms can be assigned to the bridging points between monomer units. The results are in accordance with the proposed structure of PDA, wherein the units are covalently linked by C–C bonds.<sup>[19]</sup> Fourier transform infrared spectroscopy (FTIR) also clearly confirms the formation of PDA (Figure S5). The broad peak centered at 1600 cm<sup>-1</sup> was assigned to C=C resonance vibrations in aromatic rings. A clear shoulder peak at 1715 cm<sup>-1</sup> can be ascribed to C=O groups, thus indicating the presence of quinone groups.<sup>[20]</sup> Based on the characterization results, we propose a possible structure of PDA through a slight modification of previous model,<sup>[19]</sup> wherein 5,6-hydroxyindole and 5,6-indolequinone units were covalently linked by C–C bonds between benzene rings (Scheme S1).

X-ray photoelectron spectroscopy (XPS) was used to analyze the detailed chemical composition of PDA (Figure S6). According to the curve fitting of the O1s spectra (Figure 1a), the sample R-PDA, which was synthesized without oxidation by APS and heat treatment, has only

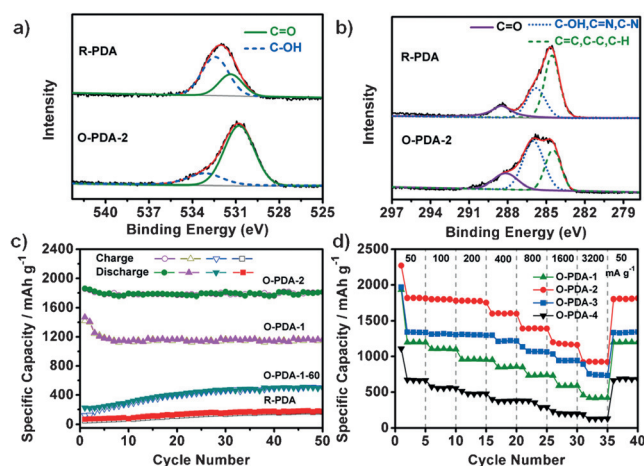


**Figure 1.** a) O1s XPS spectra of PDA samples. b) C1s XPS spectra of PDA samples. c) Comparison of cycling performances of PDA samples. d) Comparison of rate performances of PDA samples.

33.3% quinone content, while the quinone content of O-PDA-2 increased to 78.8% (Table S1). At the same time, the samples were prepared by oxidation and heat treatment all have a lower catechol content. The reduced C–OH content means the catechol has been oxidized to *o*-benzoquinone, thus resulting in a quinone-rich PDA.<sup>[17]</sup> These conclusions can also be confirmed by the C1s spectra (Figure 1b; Table S2),<sup>[20]</sup> wherein the proportion of C=O units rises as the oxidation state increases. The N 1s spectrum (Figure S6) contains only one signal (399.4 eV), which is typical for amine NH units, thus demonstrating that the amine group is connected to the aromatic ring and forms an indole structure. These results not only confirm the structure of the products, but also substantiate the assumption that the oxidant-induced polymerization of DA and heat treatment will improve the quinone contents of PDA.

We hypothesized that samples of PDA with more quinone groups would demonstrate better electrochemical performances, that is, the capacity and rate performance of the PDA would be influenced by heat treatment and the oxidant-induced polymerization process. In order to investigate the influence of these two factors on battery performance, and identify the optimized oxidation state, we carried out a series of comparison experiments. For the samples that did not undergo oxidation and heat treatment, the capacity of R-PDA was sustained at 159 mAh g<sup>-1</sup> after 50 cycles; whereas O-PDA-1-60 achieved 500 mAh g<sup>-1</sup> (through oxidant polymerization but heat treatment at only 60 °C; Figure S7a, b). Interestingly, both of O-PDA-1-60 and R-PDA present a gradual increase in capacity as the cycle number increases (Figure 1c).<sup>[5a]</sup> This phenomenon can be ascribed to the slow activation of the electrode materials with more reaction sites

during the charge/discharge process. However, this situation does not occur for O-PDA-1. For the sample of O-PDA-1 that was obtained from thermal treatment of O-PDA-1-60 at 180 °C for 24 h, the slow activation of electrode materials disappeared a remarkable improvement in capacity was observed. The reversible capacity of O-PDA-1 reaches 1180 mAh g<sup>-1</sup> and become stable after the tenth cycle. As shown in Figure 1d, the comparison of rate performance of different PDA samples clearly demonstrates the influence of the oxidant. After trying different APS/DA ratios in the synthesis, the optimized APS/DA molar ratio was 2:1, and the PDA electrodes exhibited the highest charge capacity at 1818 mAh g<sup>-1</sup>. Further increases of the molar ratio to 3:1 and 4:1 resulted in a low charge capacity for LIBs (Figure S7d,e). Such an enhanced performance might not only be attributed to the presence of the quinone group, but also can be explained by the oxidation state of PDA. It is widely accepted that polymers in full oxidation states are very unstable compared to partially doped polymers, thus indicating that O-PDA-2 has an optimal oxidation state, and thus exhibits the best electrochemical performance.

Given the adhesive ability of PDA,<sup>[14]</sup> all the coin cells in our work were composed only of PDA and conductive carbon without additional binder. As shown in Figure 2a, the specific

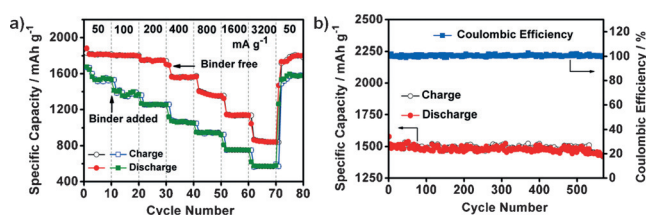


**Figure 2.** Electrochemical performance for O-PDA-2 as anode for LIBs: a) Comparison of rate performance of PDA samples in the absence and presence of binder. b) Long-term cycling profiles at a current density of 500 mA g<sup>-1</sup>.

capacity and rate performance are not optimal when polymer binder was added to the electrode, wherein the maximum capacity was only 1540 mAh g<sup>-1</sup>. When the polymer binder was added to the electrode, its capacity was lower than the binder-free battery with the same current density. The capacity fading is not so obvious in the rate performance of O-PDA-2 without polymer binder. Relative to the maximum capacity of 1818 mAh g<sup>-1</sup> at 50 mA g<sup>-1</sup>, the capacity retentions are 98 %, 96 %, 86 %, 76 %, 62 %, and 47 % at increased current density of 100, 200, 400, 800, 1600, and 3200 mA g<sup>-1</sup>, respectively (Figure 2a). We ascribe the outstanding rate performance mainly to the fast redox kinetics of *o*-benzoquinone groups and charge transfer in PDA. According to the proposed structure of PDA, charge-transfer interactions occur between *o*-benzoquinone and catechol units.<sup>[14,19]</sup> In PDA chains, charge transfer can occur between adjacent chains where the hydroquinone units (reduced state) of one chain interact with the quinone units (oxidized state) of the adjacent chain.<sup>[19]</sup> The existence of charge-transfer interactions will contribute the movement of charge carriers through

the  $\pi$  systems, thus improving the electrical conductivity of PDA, as demonstrated by electrochemical impedance spectroscopy (Figure S9c). This result indicates that controllable partial oxidization plays a key role in balancing the proportion of redox-active carbonyl groups and the conductivity.

Figure 2b shows the long-term cycling performance of O-PDA-2 at a current density of 500 mA g<sup>-1</sup>. The reversible capacity is as high as 1510 mAh g<sup>-1</sup> and remained at 1414 mAh g<sup>-1</sup> after 580 cycles with a capacity retention of 93 %. According to previous reports, catechols are gradually converted to *o*-benzoquinones during redox cycling, which indicates that (dis)charging process will improve the efficiency of redox reactions between catechols and *o*-benzoquinones, thus guaranteeing long-term cycling.<sup>[11]</sup> The good cycling performance indicates that the PDA electrode is stable in the electrolyte during the charge/discharge process. When the sample is compared before and after cycling tests, the microsphere morphology of PDA is still maintained (Figure S10). The electrode foil is insoluble in the electrolyte even after cycling tests (Figure S11), and these results not only confirm the stable cycling performance but also demonstrate the strong adhesive ability of PDA when acting as a binder material. Additionally, the function of the binder can also be supported when a typical polymer binder (such as PTFE and PVDF) was replaced by the PDA in the preparation of the electrode foil (Figures S12–S14).

SIBs have been recognized as an ideal alternative to LIBs in recent years because of the more abundant resources of sodium.<sup>[1,22]</sup> The electrochemical performance of PDA as anode materials for SIBs have also been tested. The discharge/charge profiles and CV curves of SIBs are similar to those of LIBs (Figure S15), thus indicating their similar electrochemical behavior. The initial discharge and charge capacities of the PDA electrode are 1081 and 581 mAh g<sup>-1</sup> (Figure 3a). The observed irreversible capacity results from the reaction between sodium ions and surface functional groups, as well as with the electrolyte to form a solid electrolyte interphase (SEI) layer. Fortunately, the coulombic efficiency of the PDA electrode increases dramat-

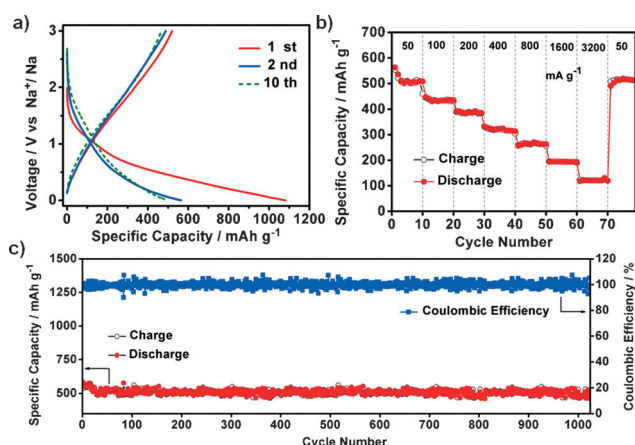


**Figure 3.** Electrochemical performance for O-PDA-2 as SIBs anode: a) Discharge/charge profiles at a current density of 50 mA g<sup>-1</sup>. b) Rate performance. c) Long-term cycling profiles at a current density of 50 mA g<sup>-1</sup>.

ically upon cycling, and reaches nearly 100% after five cycles. The discharge capacity become stable and reaches  $508 \text{ mAh g}^{-1}$  with a coulombic efficiency of nearly 100%, even after 1024 cycles at a current density of  $50 \text{ mA g}^{-1}$  (Figure 3c). As shown in Figure 3b, the O-PDA-2 electrode delivers reversible capacities of 433, 385, 323, 265, 192, and  $122 \text{ mAh g}^{-1}$  at current densities of 100, 200, 400, 800, 1600, and  $3200 \text{ mA g}^{-1}$ , respectively. As the current density drops to  $50 \text{ mA g}^{-1}$ , a reversible capacity ( $500 \text{ mAh g}^{-1}$ ) can be recovered even after 70 cycles. Such a high capacity and cycling stability have rarely reported for organic electrode materials (Tables S3, S4).

To gain insight into the structural evolution of O-PDA-2 and present a reasonable explanation for the outstanding performance, we performed theoretical calculations (Figures S18–S21, Tables S5–S7). The stabilization energy ( $\Delta E$ ) profiles of PDA unit are shown in Figure 4a. The calculated  $\Delta E$  values indicate that  $\text{Li}^+$  is favorably bound with the carbonyl oxygen atom. This conclusion is supported by ex situ spectroscopic analyses. As shown in the ex situ FTIR spectrum (Figure 4b), before the electrochemical test, the

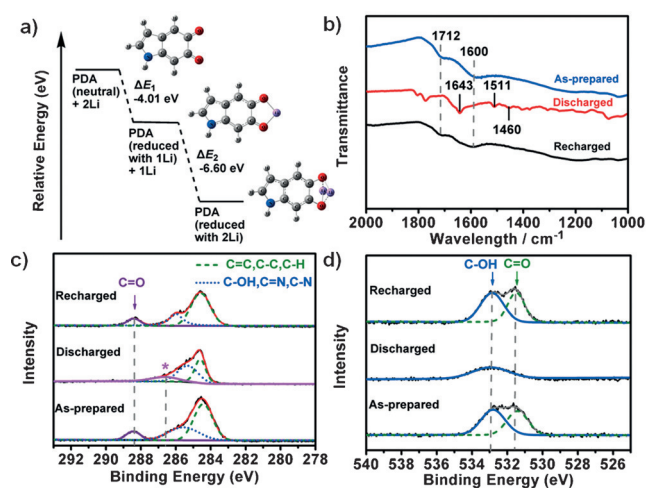


**Figure 4.** Structural evolution of O-PDA-2 as LIB anode: a) Stabilization energies of PDA unit by DFT calculations (B3LYP/6-31G(d)).  $\Delta E$  (for 1Li) =  $\Delta E_1 = E(\text{PDA-1Li}) - E(\text{PDA}) - E(\text{Li})$  and  $\Delta E$  (for 2Li) =  $\Delta E_2 = E(\text{PDA-2Li}) - E(\text{PDA-1Li}) - E(\text{Li})$ , where  $E(\text{PDA-2Li})$ ,  $E(\text{PDA-1Li})$ ,  $E(\text{PDA})$  and  $E(\text{Li})$  denote the total energies of PDA-2Li complex, PDA-1Li complex, neutral PDA, and the Li atom, respectively. b) Ex situ FTIR characterizations. c) Ex situ XPS local-scan spectra of C 1s regions. d) Ex situ XPS local-scan spectra of O 1s regions.

broad peak centered at  $1600 \text{ cm}^{-1}$  is assigned to ring ( $\text{C}=\text{C}$ ) stretching modes. The vibration at  $1712 \text{ cm}^{-1}$  is assigned to quinone groups. After discharging to 0 V, all of these features disappeared, except the signal at  $1511 \text{ cm}^{-1}$ , which corresponds to the stretching of benzene ring. This result indicates that the participation of quinone groups in the discharge reaction and the recovery of the benzene ring after the  $\text{C}=\text{O}$  bonds coordinating to  $\text{Li}^+$  ions (Figure S21).<sup>[12]</sup> After charging to 3.0 V, owing to the oxidation reaction and further formation of  $\text{C}=\text{O}$ , the broad peak around at  $1600 \text{ cm}^{-1}$  recovers. In addition, the strong vibration centered at

$1643 \text{ cm}^{-1}$  is observed in the discharged state. This peak can be ascribed to the  $\text{C}=\text{C}$  vibration in the indole ring.<sup>[23]</sup> Recent reports have also demonstrated that the aromatic amine functional groups in eumelanin offer a large distribution of binding sites for sodium ions,<sup>[9a]</sup> which indicates that the aromatic amine groups in PDA also contribute to the energy storage. The participation of aromatic amine groups during cycling is also supported by the reversible changes of the  $\text{C}-\text{NH}$  vibration (Figure S17). In addition to the *o*-benzoquinone and aromatic amines, condensed aromatic structures also contribute a proportion of the capacity. The peak intensity around  $1460 \text{ cm}^{-1}$  in the fully discharged state can be attributed to the aromatic  $\nu(\text{C}=\text{C})$  vibration modes. This signal is expected to represent the formation of an ionic complex composed of lithium ions and aromatic rings, with the negative charges in the aromatic polymer backbone.<sup>[5,24,25]</sup>

Figure 4c, d shows the ex situ XPS spectroscopic analyses. The peak located at 288.6 eV ( $\text{C}=\text{O}$ ) disappeared when discharged to 0 V (Figure 4c), thus indicating the consumption of carbonyl groups. Meanwhile, a new broadening peak at 286.6 eV emerges (marked with an asterisk). In the O 1s spectrum (Figure 4d), the peak corresponding to the carbonyl oxygen atom centered at 531.4 eV also disappeared in the discharged state, and the peak corresponding to the catechol C-OH group becomes broaden and weaker at the same time. Peak broadening occurs for the discharged electrode, thus implying the formation of a new bond between the oxygen and lithium species.<sup>[8]</sup> When recharged to 3.0 V, these processes can be reversed; all of these peaks recover to the original state. The reversible change in the  $\text{C}=\text{O}$  vibration mode effectively demonstrates the participation of *o*-benzoquinone during cycling.

In summary, to meet the challenge of current electrode materials that rely on unsustainable materials mostly from limited mineral resources, we fabricated a biodegradable bifunctional electrode based on PDA. This electrode exhibits superior electrochemical performance, including a high capacity ( $1818 \text{ mAh g}^{-1}$  for LIBs and  $500 \text{ mAh g}^{-1}$  for SIBs) and a stable cyclability (93% capacity retention after 580 cycles for LIBs; 100% capacity retention after 1024 cycles for SIBs). Detailed spectroscopic analyses were employed for structural elucidation and demonstrate that oxidant-induced polymerization and heat treatment contribute to improving the electrochemical performance of PDA, which is much better than those of state-of-the-art organic electrode materials. We believe that these findings not only provide a strategy to utilize biomolecule-derived materials, but also inspire researchers to explore high-performance and sustainable electrode materials found in the natural world. The establishment of a biomolecule-derived bifunctional electrode/binder material is a precursor for development of other versatile, sustainable, and biocompatible energy-storage systems.

## Acknowledgements

This work is financially supported by the 100 Talents Program of the Chinese Academy of Sciences, the National Program on Key Basic Research Project of China (973 program, grant

number 2012CB215500), and the National Natural Science Foundation of China (grant numbers 21271168 and 21422108).

**Keywords:** electrochemistry · lithium-ion batteries · organic electrodes · polydopamine · sodium-ion batteries

**How to cite:** *Angew. Chem. Int. Ed.* **2016**, *55*, 10662–10666  
*Angew. Chem.* **2016**, *128*, 10820–10824

- 
- [1] D. Larcher, J. M. Tarascon, *Nat. Chem.* **2015**, *7*, 19–29.  
[2] Z. Song, H. Zhou, *Energy Environ. Sci.* **2013**, *6*, 2280–2301.  
[3] Z. Song, T. Xu, M. L. Gordin, Y.-B. Jiang, I.-T. Bae, Q. Xiao, H. Zhan, J. Liu, D. Wang, *Nano Lett.* **2012**, *12*, 2205–2211.  
[4] X. Wu, J. Ma, Q. Ma, S. Xu, Y. S. Hu, Y. Sun, H. Li, L. Chen, X. Huang, *J. Mater. Chem. A* **2015**, *3*, 13193–13197.  
[5] a) J. Wu, X. Rui, G. Long, W. Chen, Q. Yan, Q. Zhang, *Angew. Chem. Int. Ed.* **2015**, *54*, 7354–7358; *Angew. Chem.* **2015**, *127*, 7462–7466; b) J. Wu, X. Rui, C. Wang, W.-B. Pei, R. Lau, Q. Yan, Q. Zhang, *Adv. Energy Mater.* **2015**, *5*, 1402189.  
[6] W. Guo, Y. X. Yin, S. Xin, Y. G. Guo, L. J. Wan, *Energy Environ. Sci.* **2012**, *5*, 5221–5225.  
[7] a) P. Hu, H. Wang, Y. Yang, J. Yang, J. Lin, L. Guo, *Adv. Mater.* **2016**, *28*, 3486–3492; b) H. Wang, P. Hu, J. Yang, G. Gong, L. Guo, X. Chen, *Adv. Mater.* **2015**, *27*, 2348–2354; c) H. Wang, F. Li, B. Zhu, L. Guo, Y. Yang, R. Hao, H. Wang, Y. Liu, W. Wang, X. Guo, X. Chen, *Adv. Funct. Mater.* **2016**, *26*, 3472–3479; d) Y. Yang, H. Wang, R. Hao, L. Guo, *Small* **2016**, DOI: 10.1002/sml.201503924.  
[8] M. Lee, J. Hong, D. H. Seo, D. H. Nam, K. T. Nam, K. Kang, C. B. Park, *Angew. Chem. Int. Ed.* **2013**, *52*, 8322–8328; *Angew. Chem.* **2013**, *125*, 8480–8486.  
[9] a) Y. J. Kim, A. Khetan, W. Wu, S. E. Chun, V. Viswanathan, J. F. Whitacre, C. J. Bettinger, *Adv. Mater.* **2016**, *28*, 3173–3180; b) Y. J. Kim, W. Wu, S. E. Chun, J. F. Whitacre, C. J. Bettinger, *Proc. Natl. Acad. Sci. USA* **2013**, *110*, 20912–20917.  
[10] D. L. Robinson, A. Hermans, A. T. Seipel, R. M. Wightman, *Chem. Rev.* **2008**, *108*, 2554–2584.  
[11] Y. J. Kim, W. Wu, S. E. Chun, J. F. Whitacre, C. J. Bettinger, *Adv. Mater.* **2014**, *26*, 6572–6579.  
[12] T. Nokami, T. Matsuo, Y. Inatomi, N. Hojo, T. Tsukagoshi, H. Yoshizawa, A. Shimizu, H. Kuramoto, K. Komae, H. Tsuyama, J. i. Yoshida, *J. Am. Chem. Soc.* **2012**, *134*, 19694–19700.  
[13] I. Kovalenko, B. Zdyrko, A. Magasinski, B. Hertzberg, Z. Milicev, R. Burtovyy, I. Luzinov, G. Yushin, *Science* **2011**, *334*, 75–79.  
[14] Y. Liu, K. Ai, L. Lu, *Chem. Rev.* **2014**, *114*, 5057–5115.  
[15] R. Ouyang, J. Lei, H. Ju, *Chem. Commun.* **2008**, 5761–5763.  
[16] W. Zheng, H. Fan, L. Wang, Z. Jin, *Langmuir* **2015**, *31*, 11671–11677.  
[17] R. Luo, L. Tang, S. Zhong, Z. Yang, J. Wang, Y. Weng, Q. Tu, C. Jiang, N. Huang, *ACS Appl. Mater. Interfaces* **2013**, *5*, 1704–1714.  
[18] Q. Wei, F. Zhang, J. Li, B. Li, C. Zhao, *Polym. Chem.* **2010**, *1*, 1430–1433.  
[19] J. Liebscher, R. Mrowczynski, H. A. Scheidt, C. Filip, N. D. Hadade, R. Turcu, A. Bende, S. Beck, *Langmuir* **2013**, *29*, 10539–10548.  
[20] R. A. Zangmeister, T. A. Morris, M. J. Tarlov, *Langmuir* **2013**, *29*, 8619–8628.  
[21] D. Dreyer, R. D. J. Miller, B. D. Freeman, D. R. Paul, C. W. Bielawski, *Langmuir* **2012**, *28*, 6428–6435.  
[22] X. Xinag, K. Zhang, J. Chen, *Adv. Mater.* **2015**, *27*, 5343–5364.  
[23] Z. Cai, G. Yang, *Synth. Met.* **2010**, *160*, 1902–1905.  
[24] X. Han, G. Qing, J. Sun, T. Sun, *Angew. Chem. Int. Ed.* **2012**, *51*, 5147–5151; *Angew. Chem.* **2012**, *124*, 5237–5241.  
[25] M. Hara, A. Satoh, N. Takami, T. Ohsaki, *J. Phys. Chem.* **1995**, *99*, 16338–16342.

Received: May 9, 2016

Published online: August 2, 2016